ELSEVIER

International Journal of Mass Spectrometry 220 (2002) 31–51

International Journal of Mass Spectrometry

www.elsevier.com/locate/ijms

A time-of-flight mass spectrometry study of the fragmentation of valence shell ionised benzene

D.M.P. Holland[a,*], D.A. Shaw[a], I. Sumner[a], M.A. Bowler[a], R.A. Mackie[b], L.G. Shpinkova[c], L. Cooper[d], E.E. Rennie[d,e], J.E. Parker[d], C.A.F. Johnson[d]

[a] *Synchrotron Radiation Department, Daresbury Laboratory, Daresbury, Warrington, Cheshire WA4 4AD, UK*
[b] *Department of Pure and Applied Physics, The Queen's University of Belfast, Belfast BT7 1NN, UK*
[c] *Department of Nuclear Spectroscopy Methods, Institute of Nuclear Physics, Moscow State University, Moscow 119899, Russia*
[d] *Department of Chemistry, Heriot-Watt University, Riccarton, Edinburgh EH14 4AS, UK*
[e] *Department of Surface Physics, Fritz-Haber Institute, Faradayweg 4-6, D-14195 Berlin, Germany*

Received 29 January 2002; accepted 28 June 2002

Abstract

A time-of-flight mass spectrometry study has been carried out to investigate the fragmentation processes occurring in benzene as a result of valence shell photoionisation. Special emphasis has been placed on high energy reactions which lead to the formation of small energetic fragments. Synchrotron radiation has been used to record spectra in the photon energy range ~14–38 eV, and appearance energies have been determined for 20 fragment ions. The time-of-flight mass spectrometer has been designed such that the collection efficiency is independent of the fragment ion initial kinetic energy and mass. This feature has enabled reliable ion yield curves to be measured. Absolute photoionisation partial cross-sections for particular fragments have been obtained by combining the ion yield curves with the absolute photoionisation cross-section. The charge separation reaction: $C_6H_6^{2+} \rightarrow CH_3^+ + C_5H_3^+$ has been observed and the appearance energy has been measured as 27.8 eV. Fragmentation rates have been determined by comparing the asymmetric time-of-flight peak shape of the $C_3H_3^+$ fragment with the corresponding data obtained by ion trajectory modelling. (Int J Mass Spectrom 220 (2002) 31–51)

Keywords: Time-of-flight mass spectrometry; Absolute photoionisation cross-sections; Charge separation reactions; Fragmentation rates

1. Introduction

In recent years, photoelectron–photoion coincidence (PEPICO) techniques, where the parent ion internal energy is defined through a measurement of the photoelectron kinetic energy, have been applied widely to the investigation of unimolecular decay processes in polyatomic ions [1–3]. The experimental information obtained in such studies includes breakdown curves, fragment ion kinetic energy release distributions and decay rates, and the majority of these results has been interpreted successfully using statistical theories of mass fragmentation [1,4–6]. An alternative means of producing internal energy selected parent ions is through multiphoton ionisation [7]. However, the energy range over which the parent ions can be formed may be restricted by the available lasers. Lately, pulsed field ionisation

* Corresponding author. E-mail: d.m.p.holland@dl.ac.uk

1387-3806/02/$ – see front matter
PII S1387-3806(02)00824-2

photoelectron–photoion coincidence spectroscopy has been performed using synchrotron radiation [8] and a resolution of better than 1 meV has been achieved.

Despite the numerous successful studies performed with the aforementioned techniques, there remain several aspects of molecular photoionisation and decay that can best be investigated using a simpler experimental approach combined with synchrotron radiation. The extended photon energy range facilitated by synchrotron radiation allows fragmentation processes having high activation energies to be examined. However, the use of synchrotron radiation is not the only requirement which needs to be satisfied in order to observe these high energy processes. Of equal importance is the capability of the spectrometer to detect the ensuing fragment ions. These fragments are often light ions and may possess kinetic energies amounting to several electron volts. Consequently, the design of the spectrometer must be such that the ion detection efficiency is independent of both the fragment mass and kinetic energy.

Threshold photoelectron–photoion coincidence (TPEPICO) spectroscopy, combined with pulsed field extraction [9], enables energetic fragments to be detected with high mass resolution. However, the time interval between the initial formation of the threshold photoelectron–photoion pair, and the application of the ion extraction field is typically 0.5–1.0 μs [10]. This delay can result in the loss of energetic fragments from the source region which, in turn, will affect the experimental breakdown curves [11]. Such losses may be particularly severe for high energy fragmentation processes and can be quantified only through detailed ion trajectory simulations [10].

In conventional, non-pulsed, time-of-flight (TOF) mass spectrometry, an analysis of the peak shape yields information about the dissociation rate and about the energy released in the form of kinetic energy during fragmentation. Such analyses have been carried out in studies using multiphoton ionisation [12,13], and have allowed the energy dependence of the unimolecular decay rate to be determined. Information of this type is more difficult to obtain with pulsed field extraction but can be deduced with a reflectron TOF spectrometer [14].

In the present work, a TOF mass spectrometer employing only static electric fields has been used to study fragmentation in benzene. Results obtained with this spectrometer for toluene [15], furan [16], pyrrole [17] and nitrobenzene [18] have already been reported, but details of the apparatus have not yet been published. Synchrotron radiation is used as the ionising source and the emphasis is placed on fragmentation processes occurring at high photon energies. The aim is to record ion yield curves that are free from discrimination for all fragments following valence shell ionisation. These curves may then be combined with the total absolute photoionisation cross-section [19] to obtain the absolute partial cross-section for a specific fragment ion. The earlier investigations [15–18] demonstrated that the present apparatus may be used to observe small fragment ions and to derive the corresponding appearance energies. For example, in all four molecules [15–18] the relative abundance curves for H^+ were measured as a function of photon energy, and these enabled, previously unknown, appearance energies to be determined.

Most previous studies investigating the unimolecular decomposition of benzene ions have concentrated on the four primary fragmentation channels occurring at low energies, namely

$$C_6H_6^+ \rightarrow C_6H_5^+ + H \quad (1)$$

$$C_6H_6^+ \rightarrow C_6H_4^+ + H_2 \quad (2)$$

$$C_6H_6^+ \rightarrow C_4H_4^+ + C_2H_2 \quad (3)$$

$$C_6H_6^+ \rightarrow C_3H_3^+ + C_3H_3 \quad (4)$$

Rosenstock et al. [20] have summarised in detail the early work using electron impact, charge exchange and single-photon absorption methods, and therefore only those studies of direct relevance to the present investigation will be discussed here.

The early breakdown curves and rate constants obtained for internal energy selected benzene ions [21–23] suggested that the rates of formation of

$C_6H_5^+$ and $C_6H_4^+$ were different. This finding was investigated further by Rosenstock et al. [24,25] who concluded that two independent pairs of competing reactions were involved, with one pair of reactions ((1) and (2)) producing $C_6H_5^+$ and $C_6H_4^+$ through H-loss, whilst the second pair ((3) and (4)) led to the formation of $C_3H_3^+$ and $C_4H_4^+$. In a later PEPICO experiment, Baer et al. [26] measured the absolute fragmentation rates for 2,4- and 1,5-hexadiyne, and the results showed that the decay rates were identical and equal to that measured previously for benzene. This indicated that all three isomers rearranged to a common ion structure prior to dissociation. An explanation for these experimental observations has been proposed by van der Hart [27]. Coincidence techniques have also been used by Braitbart et al. [28] to study slow dissociation reactions in a reflectron mass spectrometer and, in particular, single and two-step dissociation pathways were identified.

The statistical nature of the $C_6H_6^+$ dissociation was finally confirmed in a series of experiments using resonantly enhanced two-photon ionisation to produce energy selected benzene cations [29–31]. The decay rate constants for reactions (1)–(4) were measured in the energy range 5.1–5.5 eV and it was shown that H- and C-loss dissociation occurs from a common electronic state and is competing. Moreover, the RRKM/QET assumption of total internal conversion of excited electronic states to the highly vibrationally excited ground state was found to be valid. Thus, metastable decomposition to the four competing decay channels occurs from the highly vibrationally excited $\tilde{X}^2E_{1g}$ state.

Millisecond decay rates for the H-loss channel (1), have been measured recently using ion cyclotron resonance [32,33] and a cylindrical ion trap in a TOF mass spectrometer [33]. After correction for infrared relaxation, the experimental results were found to be in good agreement with calculated values. Kim et al. [34] have investigated the photodissociation kinetics of $C_6H_6^+$ on the nanosecond timescale, and found evidence for a long-lived excited electronic state lying ~2.3 eV above the ground state.

Experimental investigations have been undertaken to study the metastable decomposition of benzene parent ions [35–37], and the work showed that such transitions in the singly charged molecular ion lead to the formation of the C_2, C_3, C_4, C_5 and C_6 groups, whilst the decay of the doubly charged species results in a variety of singly and doubly charged fragments.

2. Experimental apparatus and procedure

The ion TOF spectrometer in which the experiments were performed is shown schematically in Fig. 1, and its design has been optimised for the quantitative measurement of ion yield curves. The spectrometer was attached to a 5m normal incidence monochromator [38] mounted on beamline 3 at the Daresbury Laboratory

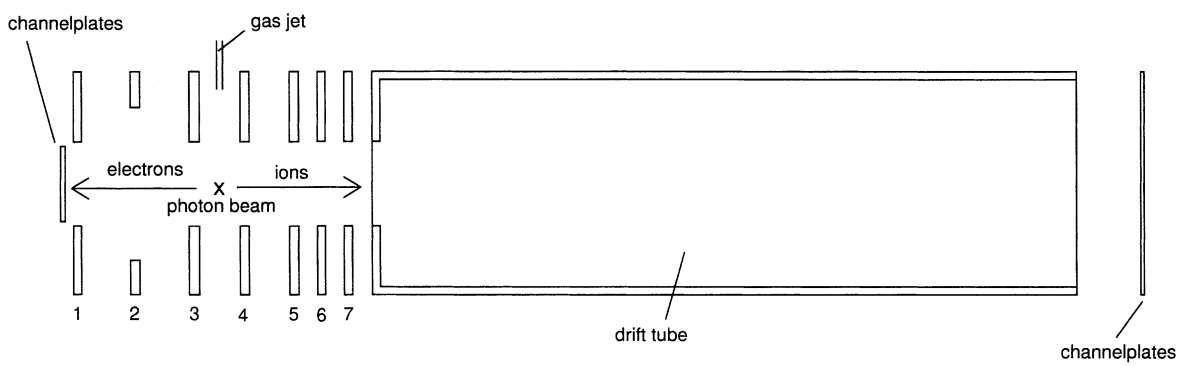

Fig. 1. A schematic representation of the ion time-of-flight mass spectrometer. Photoionisation occurs midway between plates 3 and 4, at the intersection of the photon and gas beams.

Synchrotron Radiation Source. This arrangement enabled processes occurring in the 5–40 eV range to be studied.

The diverging beam of radiation emerging from the monochromator exit slit passed into a separately pumped vacuum chamber containing an ellipsoidal mirror. This mirror focussed the radiation onto the entrance of a 2 mm bore glass capillary which then transported the radiation into the spectrometer interaction region. With this arrangement, differential pumping was provided between the spectrometer and the monochromator. Lithium fluoride, indium or tin filters could be inserted into the beam to partially suppress higher-order radiation. After passing through the interaction region the incident radiation impinged upon a sodium salicylate coated screen and the resulting fluorescence was detected with a photomultiplier. This signal could be used for normalisation purposes. At the centre of the interaction region, midway between plates 3 and 4, the radiation intersected a vertically directed beam of the gas being studied. The gas entered through an effusive nozzle mounted on an xyz manipulator, and a voltage could be applied to the nozzle to suit the source field conditions.

All the biasing voltages applied to the spectrometer plates were static, and the fields produced by these voltages were used to extract the electron–ion pairs created in the interaction region. The electrons passed

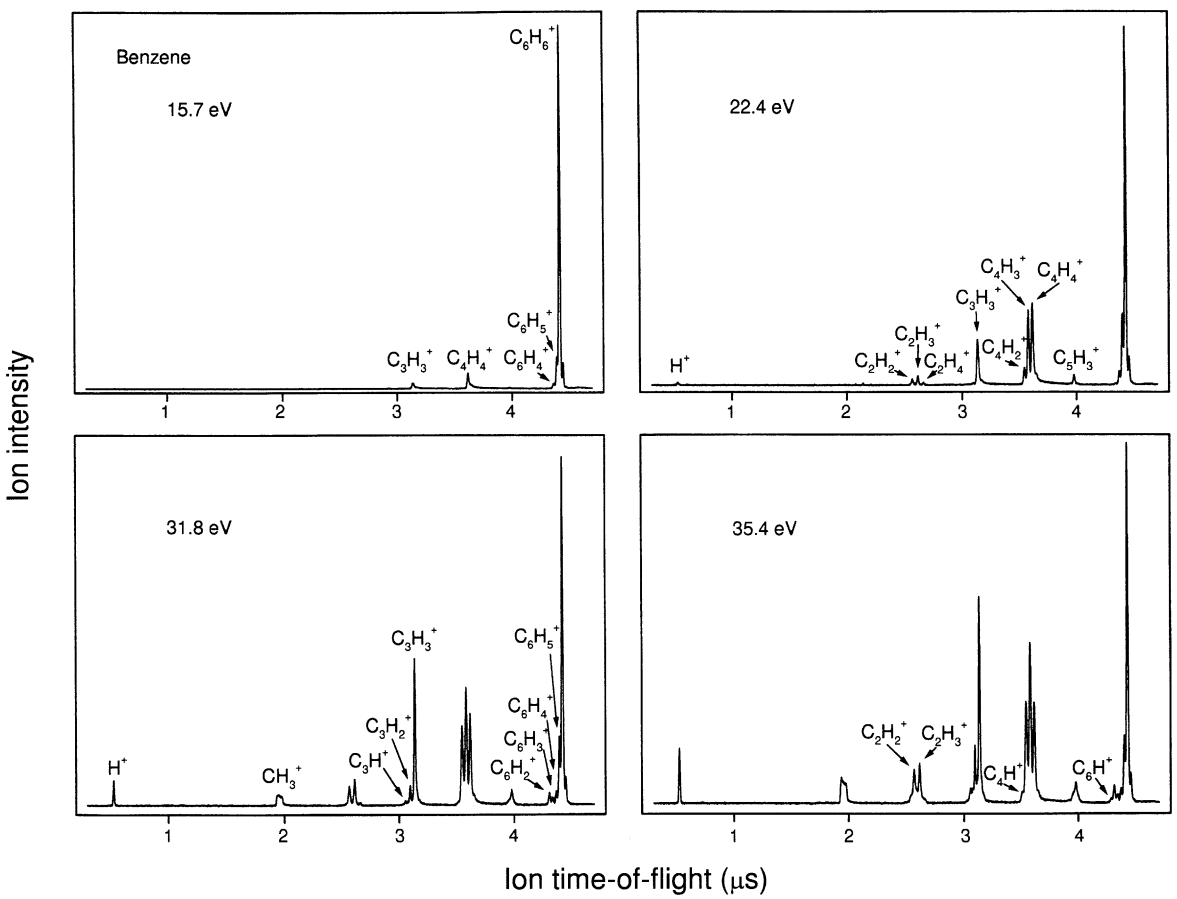

Fig. 2. Ion time-of-flight spectra of benzene recorded at photon energies of 15.7, 22.4, 31.8 and 35.4 eV.

through a simple three-element lens system and the ions through a TOF mass spectrometer. Microchannelplates were used to detect the particles, with those for the electrons being of 25 mm diameter and those for the ions being of 50 mm diameter.

The electron lens system was designed for high collection efficiency, and computer modelling using the SIMION 7 ion optics simulation program [39] showed that photoelectrons with energies up to 20 eV were collected with 100% efficiency. No kinetic energy analysis was performed as the sole purpose of the electron side was to provide the start for the ion TOF measurement. However, it was essential to ensure that the electron detection efficiency did not depend on their kinetic energy, otherwise the ion yield curves would become distorted.

The two-field TOF ion spectrometer was designed according to the criteria described by Wiley and McLaren [40], and the field strengths and geometrical factors were chosen to satisfy the spatial focussing conditions. Plates 3, 4 and 5, and plates 5, 6, 7 and 8, constitute the source field ($E_s = 300\,V\,cm^{-1}$) and the acceleration field ($E_d = 600\,V\,cm^{-1}$) regions, respectively. The k_o parameter (as defined by Wiley and McLaren) was 3.25. The detection of an ion provided the stop to the TOF measurement. The electron and ion signals were processed using standard electronics and the ion flight time was recorded using a LeCroy 4208 time-to-digital converter operating in multi-hit mode. The transmission efficiency of the TOF spectrometer was examined using SIMION, and the simulations showed that ions having kinetic energies up to 8 eV were transmitted with 100% efficiency.

As one of the objectives of the experiment was to obtain quantitatively accurate photoionisation yield curves and relative abundances, the detection efficiency of the ions by the microchannelplate detector constituted an important issue. The detector consisted of two microchannelplates mounted in a chevron configuration. Cooper et al. [41] have determined the relative detection sensitivity of a microchannelplate detector as a function of ionic mass, and their results show that the efficiency, for ions of mass greater than ~20 amu, remains essentially constant for an impact energy >7.5 keV. The mounting arrangement used in the present design allows the detector to be floated electrically such that any chosen voltage can be applied to the front face of the first channelplate whilst maintaining a constant total voltage across the two plates. TOF spectra were recorded as a function of impact energy and it was found that the peak intensity ratios showed little change for energies above 6 keV. It should also be noted that the discriminator level on the ion signal was set as low as possible, such that only very low level noise pulses were rejected.

Fig. 2 displays a selection of TOF spectra recorded at various excitation energies and it is noticeable that some of the ion peaks display asymmetric profiles. This asymmetry arises from slow dissociation (i.e., metastable) processes in which the fragment ion does not experience the full acceleration voltage. The relative abundance curves of benzene, shown in Figs. 3–8, were determined from the TOF spectra. The absolute photoionisation partial cross-section for a particular fragment ion (Figs. 9 and 10) was obtained from the product of the absolute photoionisation cross-section [19] and the corresponding relative abundance.

3. Results and discussion

3.1. Overview of the mass spectrometry studies

The TOF spectra (Fig. 2) and the relative abundance curves (Figs. 3–8) indicate that the benzene parent ion remains prominent even at high photon energies, and at 30 eV it contributes over 30% of the total ion intensity. Below 14 eV, the peak due to the $C_6H_6^+$ ion completely dominates the TOF spectra with the only other significant feature arising from the $C_6H_5^+$ fragment generated through reaction (1). Above this energy, the $C_4H_4^+$ and the $C_3H_3^+$ fragments, produced via reactions (3) and (4), begin to appear, and at higher energies the contributions due to these two ions increase rapidly. Additional fragments, such as $C_4H_3^+$ and $C_4H_2^+$, also become prominent above 20 eV.

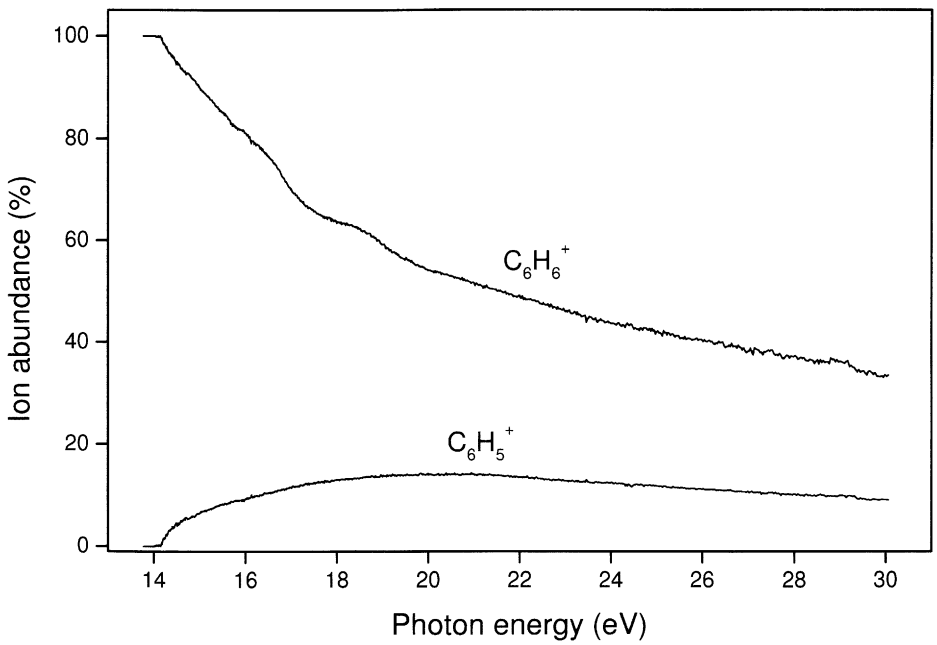

Fig. 3. Relative abundance curves for $C_6H_6^+$ ($m/z = 78$) and $C_6H_5^+$ ($m/z = 77$).

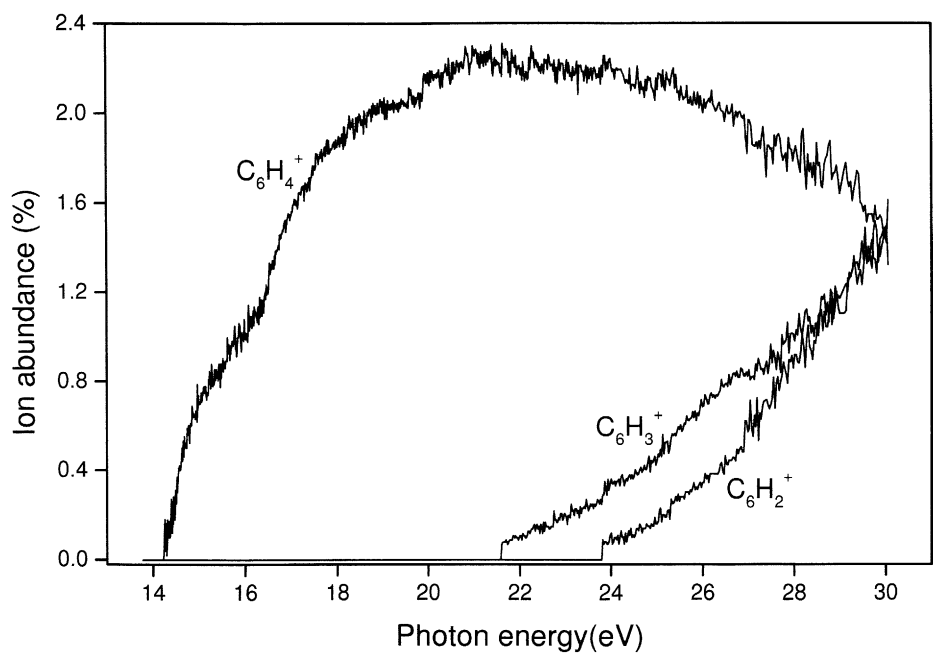

Fig. 4. Relative abundance curves for $C_6H_4^+$ ($m/z = 76$), $C_6H_3^+$ ($m/z = 75$) and $C_6H_2^+$ ($m/z = 74$).

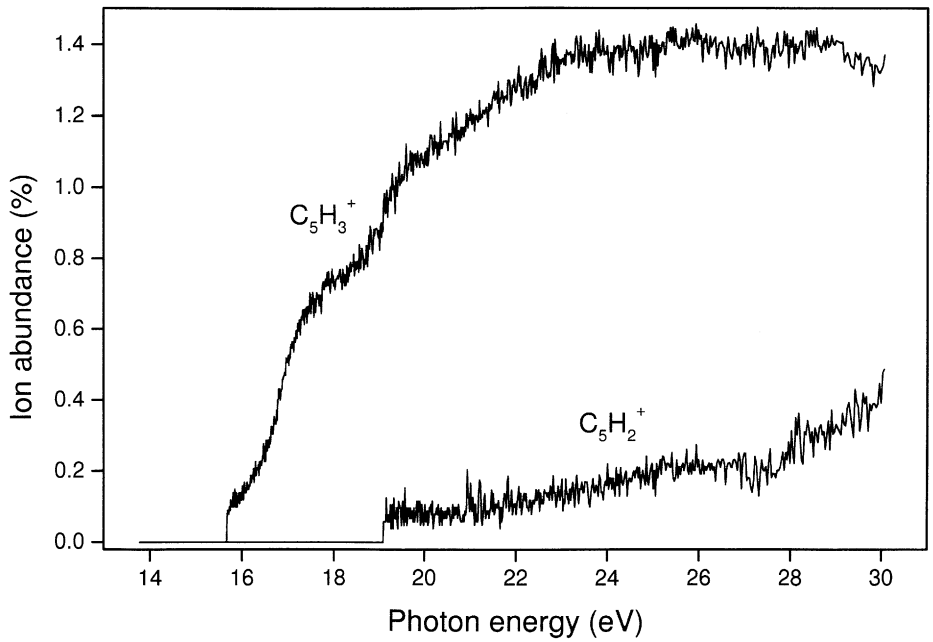

Fig. 5. Relative abundance curves for $C_5H_3^+$ ($m/z = 63$) and $C_5H_2^+$ ($m/z = 62$).

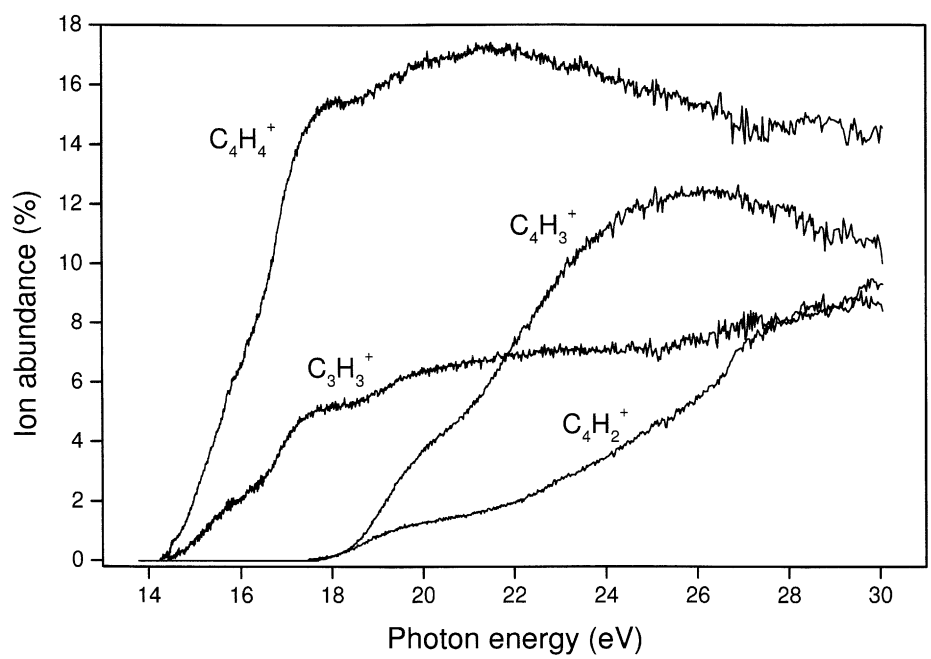

Fig. 6. Relative abundance curves for $C_4H_4^+$ ($m/z = 52$), $C_4H_3^+$ ($m/z = 51$), $C_4H_2^+$ ($m/z = 50$) and $C_3H_3^+$ ($m/z = 39$).

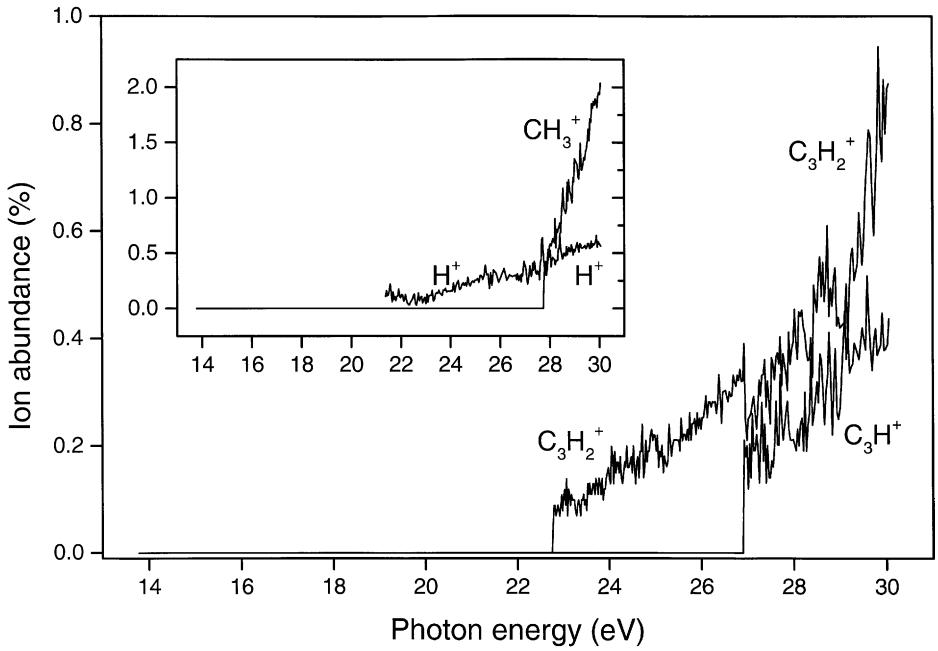

Fig. 7. Relative abundance curves for $C_3H_2^+$ ($m/z = 38$), C_3H^+ ($m/z = 37$), CH_3^+ ($m/z = 15$) and H^+ ($m/z = 1$).

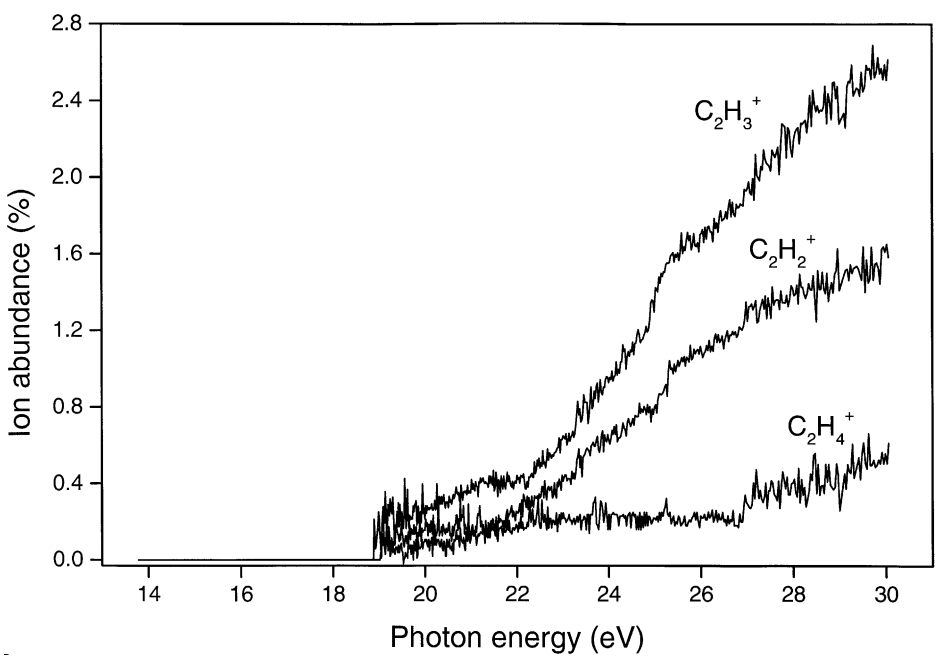

Fig. 8. Relative abundance curves for $C_2H_4^+$ ($m/z = 28$), $C_2H_3^+$ ($m/z = 27$) and $C_2H_2^+$ ($m/z = 26$).

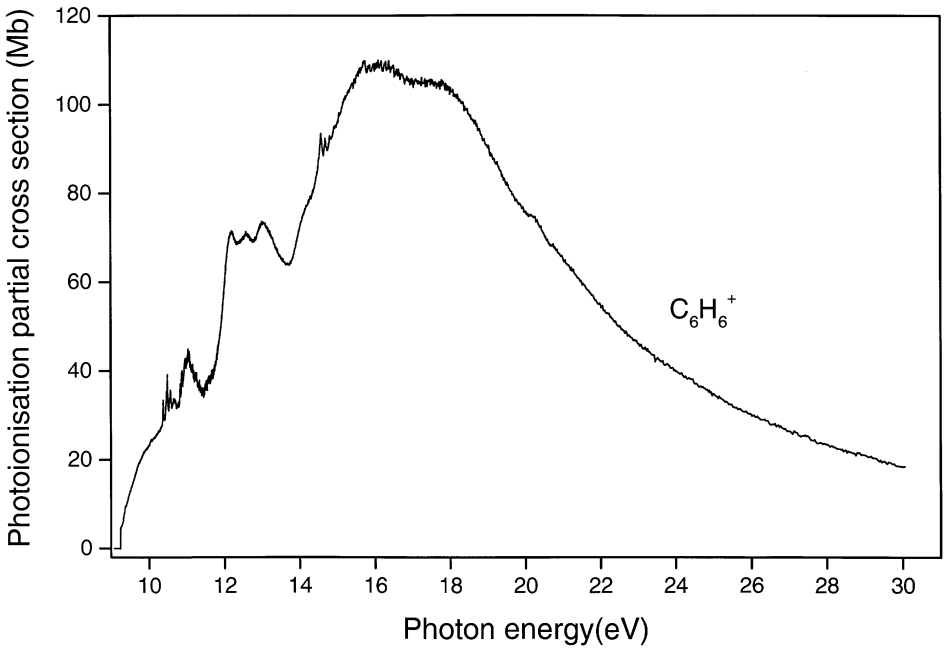

Fig. 9. The absolute photoionisation partial cross-section for the formation of $C_6H_6^+$ from benzene.

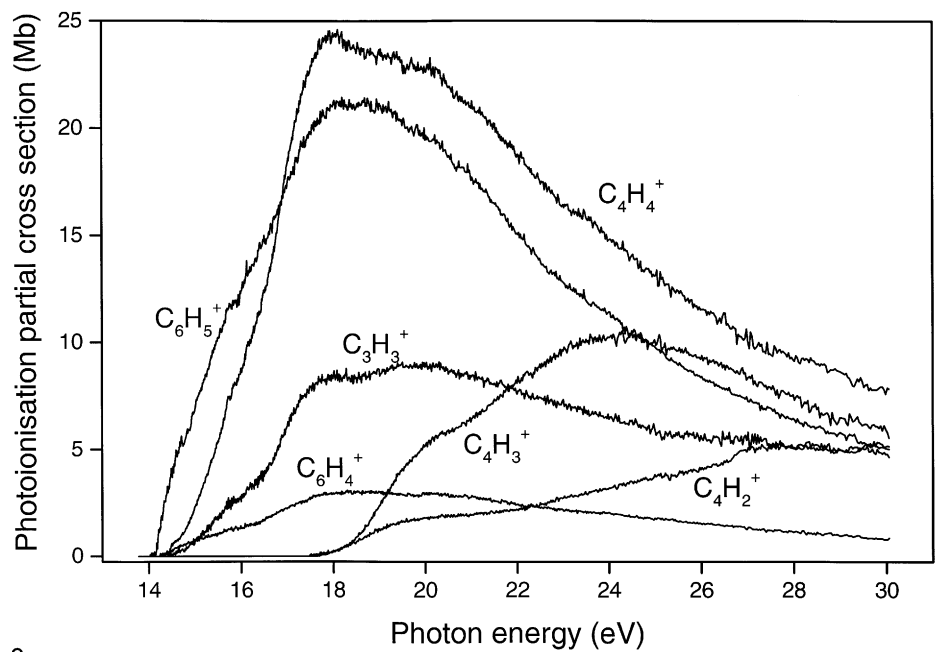

Fig. 10. The absolute photoionisation partial cross-sections for the formation of the $C_6H_5^+$, $C_6H_4^+$, $C_4H_4^+$, $C_4H_3^+$, $C_4H_2^+$ and $C_3H_3^+$ fragments from benzene.

We will discuss the fragment ions in decreasing mass order, and have provided in Table 1 a summary of the observed fragments and their AEs. Values reported in selected previous investigations have also been given. Where available, preference has been given to AEs determined in photoionisation studies, to allow a direct comparison with the present results. Also included in Table 1 are the most pertinent fragmentation processes for the formation of a particular ion, together with the associated thermochemical thresholds. These thresholds have been evaluated using the heats of formation tabulated in the NIST databases [42].

The following analysis is based primarily on a comparison between the experimentally measured AEs and the minimum energy requirement estimated from known thermochemical data. As this thermochemical estimation takes no account of the barriers in the reaction, the thresholds so obtained will always have a value lower than, or equal to, the AE. It is not unusual for such barriers, for example to a ring opening or hydrogen migration, to have energies as high as 1–2 eV. We can only estimate which fragmentation process produces the ion in question when that ion first appears. The number of accessible fragmentation channels increases as the molecular ion internal energy (or incident photon energy) increases, and it is sometimes feasible to identify the opening of a new process as a change in the gradient of the relative abundance curve. The reaction kinetics of the dissociation process are also important, and this effect will be apparent in cases where the most thermochemically favourable fragmentation is kinetically unfavourable. Under such circumstances the observed AE will be higher than expected. It should also be noted that when we estimate a heat of formation ΔH_f for an ion or neutral using our experimental AE, for those cases where the information is not readily available, the value so obtained represents an upper limit. In these cases there may be several different possible structures, and, when comparing the fragment heat of formation derived from the present work with the literature value, this should be borne in mind. For example, neutral C_3H_3 has a heat of formation of 340.6 kJ mol^{-1} for the propargyl radical and 439.3 kJ mol^{-1} for the cyclopropenyl radical.

3.2. Fragment ion appearance energies and production mechanisms

3.2.1. $C_6H_5^+$, $C_6H_4^+$, $C_6H_3^+$, $C_6H_2^+$ and C_6H^+ (m/z = 77, 76, 75, 74 and 73)

Reaction (1), which produces the phenyl cation, has the lowest energy threshold and the AE of the $C_6H_5^+$ fragment was measured as 13.80 eV. This is 0.74 eV above the thermochemical threshold. Although the formation of this fragment appears to be a simple process, involving C–H bond fission with no rearrangement of the carbon atoms, the question as to which of the low-lying electronic states of $C_6H_5^+$ is being produced has generated much debate.

Several recent theoretical investigations [32,50–52] have been carried out to study the electronic structure and dissociation energetics of the phenyl radical and cation. Agreement seems to have been reached concerning the ordering of the low-lying states, and according to Nicolaides et al. [52] the singlet ($^1A_1$) ground state of the phenyl cation has a ΔH_f of 1134 kJ mol^{-1}, whilst the triplet state ($^3B_1$) lies 103 kJ mol^{-1} higher. It should be noted that the electronic structure of the triplet phenyl cation correlates with the ground state of the benzene cation [32]. Klippenstein [50] has modelled the H-loss reaction and concludes that the phenyl cation is produced in its $^1A_1$ ground state. Thus, during the dissociation of the benzene cation, intersystem crossing occurs somewhere along the reaction coordinate. Similar conclusions were reached by Nicolaides et al. [52].

The low intensity $C_6H_4^+$ fragment ion was found to have an AE of 13.86 eV. To the best of our knowledge, the heat of formation of the $C_6H_4^+$ ion is unknown. It is evident that this fragment is formed along with molecular hydrogen as the neutral product via the low energy channel (2), instead of the alternative high energy channel which would produce two hydrogen atoms. Thus, the present data provide an upper limit of ~1420 kJ mol^{-1} for ΔH_f ($C_6H_4^+$).

Table 1
Fragment ion appearance energies and the most pertinent thermochemical thresholds

m/z	Fragments	Appearance energy (eV)		Thermochemical threshold (eV)
		Previous work	This work[a]	
77	$C_6H_5^+ + H$	12.8 [43], 12.89 [7], 13.12 [32], 13.78 [25], 13.80 [44], 13.95 [24]	13.80 ± 0.05	13.06
76	$C_6H_4^+$	12.98 [7], 13.90 [24], 14.09 [45], 14.2 [46]	13.86 ± 0.09	
75	$C_6H_3^+ + H_2 + H$	21.9 [47]	21.6 ± 0.2	16.20
	$C_6H_3^+ + 3H$			20.72
74	$C_6H_2^+ + 2H_2$	23.9 [47]	24.6 ± 0.2	15.36
	$C_6H_2^+ + H_2 + 2H$			19.88
	$C_6H_2^+ + 4H$			24.39
73[b]	C_6H^+	29 [46], 33.7 [47]	31.8 ± 0.5	
63	$C_5H_3^+$	15.7 [46], 16.8 [47]	15.69 ± 0.07	
62	$C_5H_2^+ + CH_4$	19.1 [47]	19.1 ± 0.1	11.53
	$C_5H_2^+ + CH_3 + H$			16.07
	$C_5H_2^+ + CH_2 + H_2$			16.34
	$C_5H_2^+ + CH + H_2 + H$			20.74
	$C_5H_2^+ + CH_2 + 2H$			20.85
53[b]	$C_4H_5^+$		22.1 ± 0.1	
52	(cyclo-)$C_4H_4^+ + C_2H_2$	13.37 [7], 14.17 [25]	14.22 ± 0.08	(13.69, 14.20) 14.24[c]
	(cyclo-)$C_4H_4^+ + 2CH$	14.30 [24], 14.5 [46]		(23.71, 24.20) 24.24[c]
51	$C_4H_3^+ + C_2H_3$	17.6 [46], 18.5 [47]	17.49 ± 0.08	15.4–15.7[d]
	$C_4H_3^+ + C_2H_2 + H$			16.9–17.2
	$C_4H_3^+ + C_2H + H_2$			17.3–17.6
	$C_4H_3^+ + C_2H + 2H$			21.8–22.1
	$C_4H_3^+ + CH_2 + CH$			22.5–22.8
50	$C_4H_2^+ + C_2H_4$	17.5 [46], 18.3 [47]	17.48 ± 0.08	14.41
	$C_4H_2^+ + C_2H_2 + H_2$			16.21
	$C_4H_2^+ + C_2H_3 + H$			19.22
	$C_4H_2^+ + C_2H_2 + 2H$			20.73
	$C_4H_2^+ + 2CH_2$			21.93
49[b]	C_4H^+	27.6 [47]	31.8 ± 0.5	
39	(cyclo-)$C_3H_3^+ + C_3H_3$	13.43 [7], 14.25 [24], 14.7 [46]	14.44 ± 0.06	(13.83) 14.87
	(cyclo-)$C_3H_3^+$ + cyclo-C_3H_3			(14.85) 15.90
	(cyclo-)$C_3H_3^+ + C_3H_2 + H$			(14.58) 15.63
	(cyclo-)$C_3H_3^+$ + cyclo-$C_3H_2 + H$			(15.40) 17.30
38	(cyclo-)$C_3H_2^+ + C_3H_4$	23.0 [47]	22.79 ± 0.08	(13.53) 13.07
	(cyclo-)$C_3H_2^+ + C_3H_2 + H_2$			(13.62) 13.16
	(cyclo-)$C_3H_2^+$ + cyclo-$C_3H_2 + H_2$			(14.44) 13.98
	(cyclo-)$C_3H_2^+ + C_2H_2 + CH_2$			(15.63) 15.17
	(cyclo-)$C_3H_2^+ + C_3H_3 + H$			(17.39) 16.92
	(cyclo-)$C_3H_2^+$ + cyclo-$C_3H_3 + H$			(18.41) 17.95
	(cyclo-)$C_3H_2^+ + C_3H_2 + 2H$			(18.14) 17.68
	(cyclo-)$C_3H_2^+$ + cyclo-$C_3H_2 + 2H$			(18.96) 18.50
	(cyclo-)$C_3H_2^+ + C_2H_2 + CH + H$			(20.03) 19.57
	(cyclo-)$C_3H_2^+ + C_2H_3 + CH$			(20.87) 20.41
	(cyclo-)$C_3H_2^+ + C_2H_2 + C + H_2$			(21.37) 20.91
	(cyclo-)$C_3H_2^+ + C_2H_2 + C + 2H$			(23.54) 23.08
	(cyclo-)$C_3H_2^+ + CH_2 + 2CH$			(27.98) 27.51

Table 1 (*Continued*)

m/z	Fragments	Appearance energy (eV)		Thermochemical threshold (eV)
		Previous work	This work[a]	
37	$C_3H^+ + C_3H_4 + H$	27.4 [47]	26.9 ± 0.1	16.78
	$C_3H^+ +$ (cyclo-)$C_3H_3 + H_2$			(17.14) 16.11
	$C_3H^+ + C_2H_2 + CH_3$			16.44
	$C_3H^+ +$ (cyclo-)$C_3H_2 + H_2 + H$			(17.69) 16.87
	$C_3H^+ + C_2H_3 + CH_2$			19.71
	$C_3H^+ +$ (cyclo-)$C_3H_3 + 2H$			(21.66) 20.63
	$C_3H^+ + C_2H_2 + CH + H_2$			21.11
	$C_3H^+ + C_2H_2 + CH_2 + H$			21.22
	$C_3H^+ +$ (cyclo-)$C_3H_2 + 3H$			(22.21) 21.39
	$C_3H^+ + C_2H_3 + C + H_2$			23.11
	$C_3H^+ + C_2H_3 + CH + H$			24.12
	$C_3H^+ + C_2H_2 + C + H_2 + H$			24.62
	$C_3H^+ + C_2H_2 + CH + 2H$			25.63
	$C_3H^+ + C_2H_3 + C + 2H$			27.63
	$C_3H^+ + C_2H_2 + C + 3H$			29.14
28	$C_2H_4^+ + C_4H_2$		19.0 ± 0.8	15.01
	$C_2H_4^+ +$ (cyclo-)$C_3H_2 + C$			(20.47) 19.65
	$C_2H_4^+ + 2C_2H$			19.80
27	$C_2H_3^+ + C_2H_2 + C_2H$	19 [46], 21.1 [47]	18.9 ± 0.5	17.69
	$C_2H_3^+ +$ (cyclo-)$C_3H_2 + CH$			(19.51) 18.69
	$C_2H_3^+ +$ (cyclo-)$C_3H_3 + C$			(22.47) 21.45
	$C_2H_3^+ + 2C_2H + H$			22.45
26	$C_2H_2^+ + C_4H_4$	17.9 [47], 19 [46]	18.9 ± 0.5	18.69[e], 19.13[f], 19.51[g], 20.03[h]
	$C_2H_2^+ + 2C_2H_2$			20.23
	$C_2H_2^+ +$ (cyclo-)$C_3H_3 + CH$			(26.26) 25.23
15	CH_3^+	28.2 [48]	27.8 ± 0.1	
1	H^+		<20.2	

[a] The quoted uncertainties have been based on the results obtained from the fitting procedure applied to the TOF spectra. However, if the rate constant for the production of a particular fragment ion is low at threshold, then the measured AE will be influenced by a kinetic shift. Under such circumstances the true AE may be substantially lower than the observed value. Following more detailed studies, a few of the AE values have been improved since the preliminary results were reported by Cooper et al. [18].

[b] These very low intensity fragments have not been included in the relative abundance curves.

[c] The cyclic structures are written in the order (methylenecyclopropene, cyclobutadiene). For the cyclic structures the heats of formation have been taken from Staley and Norden [49]. The planar structure in this case may be either 1-buten-3-yne ($\Delta H_f(C_4H_4^+) = 1229.7\,kJ\,mol^{-1}$) or 1,2,3-butatriene ($\Delta H_f(C_4H_4^+) = 1230.1\,kJ\,mol^{-1}$).

[d] Three different, but equally valid upper limits for the ΔH_f ($C_4H_3^+$) have been estimated (see text) hence a range of calculated thermochemical thresholds has been given.

[e] 1-Buten-3-yne, ΔH_f (C_4H_4) = $305.0\,kJ\,mol^{-1}$.

[f] 1,2,3-Butatriene, ΔH_f (C_4H_4) = $347.3\,kJ\,mol^{-1}$.

[g] Cyclobutadiene, ΔH_f (C_4H_4) = $434.3\,kJ\,mol^{-1}$ [49].

[h] Methylenecyclopropene, ΔH_f (C_4H_4) = $384.5\,kJ\,mol^{-1}$ [49].

The $C_6H_3^+$, $C_6H_2^+$ and C_6H^+ fragments gave rise to weak peaks in the TOF spectra, and their AEs were determined as 21.6, 24.6 and 31.8 eV, respectively. If a value of ~1428 kJ mol^{-1} is used for ΔH_f ($C_6H_3^+$) [18], then a thermochemical threshold of 16.2 eV is obtained for the production of $C_6H_3^+$ together with molecular hydrogen and one hydrogen atom as the neutral products, and a threshold of 20.72 eV for the formation of $C_6H_3^+$ and three hydrogen atoms. The experimental AE is in good agreement with the latter threshold.

Considering now the formation of the $C_6H_2^+$ ion, there are three possible thermochemical thresholds, at 15.36, 19.88 and 24.39 eV, where this fragment is

produced together with the neutrals $2H_2$, $H_2 + 2H$ and 4H, respectively. Of these three reactions, the channel with the highest thermochemical threshold (24.39 eV), where $C_6H_2^+$ is formed together with four hydrogen atoms, shows the closest agreement with the experimental observation. The C_6H^+ ion has a rather high AE, and since the lowest ΔH_f (C_6H^+) that can be derived from this value is over 2000 kJ mol^{-1} (corresponding to the formation of C_6H^+ and five hydrogen atoms) it appears that a substantial energy barrier must exist in this fragmentation channel.

From the above discussion, it can be seen that only the $C_6H_4^+$ ion is formed, together with molecular hydrogen, via a low energy channel, whilst the other $C_6H_n^+$ ions are produced through sequential hydrogen loss mechanisms.

3.2.2. $C_5H_3^+$ and $C_5H_2^+$ (m/z = 63 and 62)

The AEs for the low intensity fragments $C_5H_3^+$ and $C_5H_2^+$ were measured as 15.69 and 19.10 eV, respectively. As far as we are aware, a value of ΔH_f ($C_5H_3^+$) is not available. However, values of 1451, 1001, 990 and 565 kJ mol^{-1} can be derived for fragmentation channels (5)–(8), respectively,

$$C_6H_6^+ \rightarrow C_5H_3^+ + CH_3 \quad (5)$$

$$C_6H_6^+ \rightarrow C_5H_3^+ + CH + H_2 \quad (6)$$

$$C_6H_6^+ \rightarrow C_5H_3^+ + CH_2 + H \quad (7)$$

$$C_6H_6^+ \rightarrow C_5H_3^+ + CH + 2H \quad (8)$$

Channel (8) produces a heat of formation, ΔH_f ($C_5H_3^+$), which is too high to be feasible when compared to typical values for hydrocarbon ions. For example, the cyclopentadienyl radical ion has a ΔH_f ($C_5H_5^+$) of ~1054 kJ mol^{-1}, and the $C_5H_2^+$ ion, formed in the valence shell ionisation of nitrobenzene, has an upper limit of ~1270 kJ mol^{-1} for ΔH_f ($C_5H_2^+$) [18]. This indicates that the most plausible mechanism for the formation of the $C_5H_3^+$ ion from benzene involves one or two hydrogen transfers together with a ring break or rearrangement before fragmentation. Thus, the present work enables an upper limit of 1451 kJ mol^{-1} to be placed on ΔH_f ($C_5H_3^+$).

We have used the above value of 1270 kJ mol^{-1} for ΔH_f ($C_5H_2^+$) to estimate the thermochemical thresholds for the formation of $C_5H_2^+$ from the benzene ion. Table 1 indicates that there are several possible reactions, and two of the channels have thresholds which are near to the AE. The first of these channels, with an estimated threshold at 16.07 eV, is effectively reaction (5), followed by the loss of an additional hydrogen atom from the $C_5H_3^+$ fragment. A substantial energy barrier and/or unfavourable kinetics can explain the difference of ~3 eV between the experimental AE and the thermochemical threshold. Alternatively, if ΔH_f ($C_5H_2^+$) is over estimated by ~150 kJ mol^{-1}, then the higher energy channels become accessible. However, this would lead to a value of <1120 kJ mol^{-1} for ΔH_f ($C_5H_2^+$), which seems too low.

3.2.3. $C_4H_5^+$, $C_4H_4^+$, $C_4H_3^+$, $C_4H_2^+$ and C_4H^+ (m/z = 53, 52, 51, 50 and 49)

The high energy TOF spectra, shown in Fig. 2, contain three prominent peaks which can be attributed to the $C_4H_4^+$, $C_4H_3^+$ and $C_4H_2^+$ fragment ions. The peak due to the $C_4H_5^+$ fragment is much weaker, and this ion was found to have an AE of 22.1 eV. We believe that the peak attributed to the $C_4H_5^+$ fragment originates from this ion, and not from the ^{13}C isotope of the $C_4H_4^+$ fragment, because the yield curve exhibited a clear onset rather than a gradual rise. To the best of our knowledge, there is no value in the literature for ΔH_f ($C_4H_5^+$). However, values of 1738, 903 and 564 kJ mol^{-1} may be derived for fragmentation channels (9)–(11), respectively,

$$C_6H_6^+ \rightarrow C_4H_5^+ + C_2H \quad (9)$$

$$C_6H_6^+ \rightarrow C_4H_5^+ + CH + C \quad (10)$$

$$C_6H_6^+ \rightarrow C_4H_5^+ + 2C + H \quad (11)$$

Only reaction (9) yields a heat of formation which is sufficiently high to be probable. Thus, it appears that the $C_4H_5^+$ ion is formed, together with the C_2H neutral, through a process involving a substantial energy barrier and/or unfavourable kinetics.

The high intensity channel (3), which generates the $C_4H_4^+$ fragment ion along with neutral acetylene,

has an AE of 14.22 eV. Using the heats of formation reported by Staley and Norden [49], the estimated thermochemical thresholds for reaction (3) are 13.69 and 14.20 eV, depending on whether the $C_4H_4^+$ fragment is formed as the methylenecyclopropene or the cyclobutadiene radical cation, respectively. Alternatively, the $C_4H_4^+$ fragments may be formed with linear structures, and these thresholds have been estimated using the heats of formation listed in the NIST databases [42]. A thermochemical threshold of 14.24 eV has been estimated for both the 1,2,3-butatriene and the 1-buten-3-yne structures.

Ab initio calculations have been undertaken to study the possible pathways for the formation of $C_4H_4^+$ ion structures from a $C_6H_6^+$ precursor [53,54]. The work showed that the lower energy product ions have structures corresponding to methylenecyclopropene and to 1-buten-3-yne. The other possible classical structures of cyclobutadiene and 1,2,3-butatriene ions may be discounted as they involve several high energy barriers. These theoretical results are in accord with earlier experimental studies [55–57] which provided evidence that two structures, one of which was the methylenecyclopropene structure, was formed along with neutral acetylene from photoionised benzene.

The thermochemical reasoning indicates that, below ~14.2 eV, reaction (12), where the $C_4H_4^+$ fragment is formed with the cyclo structure, would be responsible for the production of this ion:

$$C_6H_6^+ \rightarrow \text{cyclo-}C_4H_4^+ + C_2H_2 \quad (12)$$

However, at the experimental AE of 14.22 eV the 1-buten-3-yne structure appears most likely.

The present AE of 14.22 eV allows a barrier height of 4.98 eV, relative to the ground state of the benzene radical cation, to be derived for the reaction producing the $C_4H_4^+$ ion fragment. This energy may be compared to computed values [54] of 4.57 eV for the channel leading to the formation of methylenecyclopropene, and of 4.92 and 4.96 eV for two slightly different routes resulting in the production of 1-buten-3-yne. The good agreement between the experimental and the calculated barriers provides support for the dissociation mechanisms proposed by van der Hart [54]. It is interesting to note that the aforementioned mechanisms involve H-atom 1,2 shifts preceding C–C bond breaking and do not proceed by a simple rupture of a pair of C–C bonds and the loss of neutral acetylene. Thus, the proposed mechanisms are similar to those invoked in describing the fragmentation processes observed in valence shell ionised furan [16] and pyrrole [17].

The AE of the $C_4H_3^+$ fragment was measured as 17.49 eV. Neither of the NIST databases [42] contains a heat of formation for this ion. However, three independent values, representing upper limits, have been published, and these vary from 1272 to 1302 kJ mol^{-1} (see Cooper et al. [18] for details). We have estimated thermochemical thresholds for a range of reactions listed in Table 1, using the minimum (1272 kJ mol^{-1}) and maximum (1302 kJ mol^{-1}) limits. The thresholds for fragmentation channels (13) and (14) lie just below the AE, which suggests that the $C_4H_3^+$ fragment could be produced through both of these mechanisms:

$$C_6H_6^+ \rightarrow C_4H_3^+ + C_2H_2 + H \quad (13)$$

$$C_6H_6^+ \rightarrow C_4H_3^+ + C_2H + H_2 \quad (14)$$

The AE of the prominent $C_4H_2^+$ fragment was found to be 17.48 eV. If it is assumed that the fragment is formed with the 1,3-butadiyne linear structure, having a ΔH_f ($C_4H_2^+$) of 1420.6 kJ mol^{-1}, then fragmentation channels (15) and (16), with thermochemical thresholds of 14.41 and 16.21 eV, respectively, are possible:

$$C_6H_6^+ \rightarrow C_4H_2^+ + C_2H_4 \quad (15)$$

$$C_6H_6^+ \rightarrow C_4H_2^+ + C_2H_2 + H_2 \quad (16)$$

The low intensity fragment ion C_4H^+ was found to have an AE of 31.8 eV. The lowest ΔH_f (C_4H^+) that can be derived from the AE is ~1800 kJ mol^{-1}, which indicates that the fragmentation process must be affected by a substantial barrier. Since the AE of $C_4H_2^+$ is ~17–18 eV, and the direct fragmentation process $C_4H_2^+ \rightarrow C_4H^+ + H$ requires only ~5–6 eV, it appears that the C_4H^+ fragment is not formed through H-loss from the $C_4H_2^+$ ion.

3.2.4. $C_3H_3^+$, $C_3H_2^+$ and C_3H^+ (m/z = 39, 38 and 37)

Reaction (4), which produces the high intensity $C_3H_3^+$ fragment, has an AE of 14.44 eV, and several fragmentation channels resulting in the formation of the $C_3H_3^+$ ion from $C_6H_6^+$ are listed in Table 1. However, only one of the channels has a threshold energy lying below the AE. This channel, with a threshold of 13.83 eV, produces the cyclopropenyl $C_3H_3^+$ ion and the propargyl C_3H_3 neutral radical.

van der Hart [58] has carried out ab initio calculations to examine the possible pathway for the formation of $C_3H_3^+$ fragment ions from the benzene radical cation. The work indicates that the highest barrier in the fragmentation of $C_6H_6^+$ to the cyclopropenyl cation is slightly lower than the total energy of the separated fragments, and amounts to ~4.88 eV. van der Hart proposes a fragmentation pathway in which the first step involves isomerisation of the benzene radical cation to the fulvene structure. Ring opening of the fulvene structure, followed by ring closure leads to the production of the allyl-cyclopropene radical cation, and the subsequent loss of the linear CH_2CCH radical results in the formation of the $C_3H_3^+$ cyclopropenyl fragment.

The present AE of 14.44 eV for the $C_3H_3^+$ fragment leads to a barrier of 5.20 eV, with respect to the ground state of the benzene radical cation. This value is in good agreement with the prediction of 4.88 eV [58]. The fitting procedure employed by Neusser [7] resulted in a significantly lower threshold value of 4.19 eV for this dissociation.

The high AE of 22.79 eV for the low intensity $C_3H_2^+$ fragment indicates that this ion is being formed via sequential decomposition processes. The relevant fragmentation processes, many of which produce molecules as the neutral products, are listed in Table 1. Of these processes, there are three mechanisms (reactions (17)–(19)) which have thermochemical thresholds between 19.57 and 21.37 eV. In each case the $C_3H_2^+$ ion can take either the propadienylidene or the cyclopropenylidene structures:

$$C_6H_6^+ \rightarrow C_3H_2^+ + C_2H_2 + CH + H \quad (17)$$

$$C_6H_6^+ \rightarrow C_3H_2^+ + C_2H_3 + CH \quad (18)$$

$$C_6H_6^+ \rightarrow C_3H_2^+ + C_2H_2 + C + H_2 \quad (19)$$

The high AE of 26.9 eV for the C_3H^+ fragment again indicates formation via sequential decomposition. If we use a ΔH_f (C_3H^+) of 1297 kJ mol^{-1}, taken from a similar study on photoionised pyrrole [17], then the most probable fragmentation reaction, with a thermochemical threshold of 25.63 eV is:

$$C_6H_6^+ \rightarrow C_3H^+ + C_2H_2 + CH + 2H \quad (20)$$

This mechanism is basically the formation of the $C_3H_2^+$ ion (reaction (17)) with the further loss of a hydrogen atom.

3.2.5. $C_2H_4^+$, $C_2H_3^+$ and $C_2H_2^+$ (m/z = 28, 27 and 26)

The relative abundance curves for the low intensity $C_2H_4^+$, $C_2H_3^+$ and $C_2H_2^+$ fragments exhibit very gradual rises in the threshold regions, with no distinct onsets being discernible. Consequently, the determination of the AEs presents difficulties and an analysis of the data suggests a threshold of 18.9 eV for $C_2H_2^+$ and $C_2H_3^+$, and a slightly higher threshold for $C_2H_4^+$.

Several fragmentation channels that lead to the formation of $C_2H_4^+$ have been listed in Table 1, and although only one of these channels has a thermochemical threshold below the AE, the thresholds for two other channels lie within the experimental uncertainty. As the energy difference between the lowest thermochemical threshold and the AE is ~4 eV, it appears likely that, at the observed onset, the $C_2H_4^+$ fragment is produced either through the channel with a thermochemical threshold at 19.65 eV, where it is formed together with linear C_3H_2 and atomic carbon neutrals, or through the channel with a thermochemical threshold at 19.80 eV, where it is formed together with two neutral molecules of C_2H.

The production of the $C_2H_3^+$ fragment may proceed through reactions (21) and (22), with thresholds of 17.69 and 18.69 eV, respectively,

$$C_6H_6^+ \rightarrow C_2H_3^+ + C_2H_2 + C_2H \quad (21)$$

$$C_6H_6^+ \rightarrow C_2H_3^+ + C_3H_2 + CH \quad (22)$$

Table 1 lists several reactions resulting in the production of the $C_2H_2^+$ fragment, but only one of these reactions (23) has thermochemical thresholds lying below the AE. There are four possible structures for the neutral C_4H_4 molecule, but only the two planar structures (1-buten-3-yne and 1,2,3-butatriene) produce thresholds within the AE uncertainty limits:

$$C_6H_6^+ \rightarrow C_2H_2^+ + C_4H_4 \quad (23)$$

3.2.6. CH_3^+ and H^+ (m/z = 15 and 1)

The CH_3^+ fragment was found to have an AE of 27.8 eV, which is substantially higher than the thermochemical threshold of 21.6 eV [59]. This suggests that a charge separation reaction, as described in Section 3.4, may be responsible for the production of the CH_3^+ fragment.

The relative abundance curve for H^+ exhibits an extremely slow rise, as a function of energy, and the AE cannot be determined with a high degree of confidence. The data indicate that the threshold for H^+ formation lies below 20.2 eV. Various neutral partners may accompany the production of this ion.

3.3. Fragment ion absolute photoionisation partial cross-sections

The absolute photoionisation partial cross-section for the production of a specific fragment ion following photoabsorption in molecular benzene can be determined from the product of the relative abundance curve for that particular fragment and the absolute photoionisation cross-section [19]. Surprisingly, in view of the numerous investigations that have been undertaken to study photoionisation phenomena in benzene, even the relative abundance curves have been measured for only the most prominent fragments [24,25]. Figs. 9 and 10 show a selection of absolute photoionisation partial cross-sections obtained from the present data, and the spectrum for $C_6H_6^+$ exhibits extensive structure, some of which can be associated with excitation into Rydberg states [19]. The spectra for the smaller fragment ions display little, or no, sharp structure but contain one or more broad features. These features have been discussed by Jochims et al. [60] in connection with the information that they provide about isomerisation, competitive dissociation channels and sequential fragmentation.

Unfortunately, Jochims et al. [60] have not published their measured fragment ion yield spectra for benzene, but only tabulated the energy (or energies) at which the spectrum for a specific fragment exhibits a maximum (or minima). Their results were as follows, where the value given after a particular fragment corresponds to the peak energy (or energies): $C_6H_6^+$ 18.4 and 20.0 eV, $C_6H_5^+$ 17.8 eV, $C_6H_4^+$ 18.3 eV, $C_4H_4^+$ 17.7 eV, $C_4H_3^+$ $\geq$22.0 eV and $C_3H_3^+$ $\geq$18.0 eV. For these same six fragments, the present data give the following peak energies: $C_6H_6^+$ 16.1 and 17.7 eV, $C_6H_5^+$ 18.5 eV, $C_6H_4^+$ 18.4 eV, $C_4H_4^+$ 17.9 eV, $C_4H_3^+$ 24.3 eV and $C_3H_3^+$ 18.0 and 20.0 eV. Although some of the peaks in the ion yield spectra are broad, it is difficult to account for the discrepancies. The peak energies depend upon three factors: (1) the absolute photoabsorption cross-section for benzene, (2) the corresponding photoionisation quantum efficiency, and (3) a complete set of relative abundance curves. Several recent measurements of the absolute photoabsorption cross-section have been compared by Rennie et al. [19], and are in reasonable agreement. Furthermore, in the relevant photon energy range, the photoionisation quantum efficiency used in the present analysis is similar to that recorded by Jochims et al. [61]. Therefore, it appears likely that the discrepancies in the peak energies observed for some of the fragment ions can be attributed to differences in the relative abundance curves. This emphasises the need to ensure that the spectrometer design is such that the ion detection efficiency is independent of both the fragment mass and kinetic energy.

Jochims et al. [60] have used benzene as a prototype polycyclic aromatic hydrocarbon molecule to illustrate the type of information about fragmentation and electronic structure that can be obtained from ion yield curves. In particular, they have used some photoelectron partial cross-sections measured by Carlson et al. [62] to predict the energy of the maximum occurring in the $C_6H_6^+$ spectrum. Their analysis rests

on the assumption that electron ejection from the three highest occupied molecular orbitals of benzene leads to the formation of $C_6H_6^+$, whilst electron ejection from the more tightly bound orbitals results in fragment ion formation. Based on their evaluation of the photoelectron data, Jochims et al. [60,61] predict that the $C_6H_6^+$ partial cross-section should display a peak at 16 eV. This prediction appeared in only fair accordance with their observed peak energy of 18.4 eV, but is in excellent agreement with the present result.

3.4. Charge separation reactions in doubly ionised benzene cations

The fragmentation of $C_6H_6^{2+}$ into two singly charged ions has been studied previously using conventional electron impact mass spectrometry [35,48,63,64] and more recently using the photoion–photoion coincidence technique [65]. This latter investigation enabled the separation of $C_6H_6^{2+}$ into three groups of ion pairs related to $C_3H_3^+ + C_3H_3^+$, $C_2H_3^+ + C_4H_3^+$ and $CH_3^+ + C_5H_3^+$ to be identified. In the present study the last of these three reactions, namely, $C_6H_6^{2+} \rightarrow CH_3^+ + C_5H_3^+$, has been observed and the kinetic energy released during the separation has been determined from an analysis of the peak shape associated with the CH_3^+ fragment.

In our study on nitrobenzene [18] a description was given of the way in which an analysis of the peak profile associated with a fragment ion could yield the initial kinetic energy possessed by that ion. This energy could then be related to the initial ion-pair separation by assuming a simple Coulomb explosion model [66]. The TOF spectra displayed in Fig. 2 show that the peak corresponding to the CH_3^+ ion is broad, and an analysis of the profile indicates that the initial translational energy possessed by the CH_3^+ fragment is 2.5 eV. Assuming that dissociation of the doubly charged parent ion produces only CH_3^+ and $C_5H_3^+$, so that no consideration needs to be given to an additional neutral fragment, then conservation of momentum results in a total kinetic energy release of 3.1 eV. This value is in very good agreement with that of 3.0 eV reported by Richardson et al. [65], and confirms that the earlier estimates were too small [35]. The appearance energy for this charge separation reaction is 27.8 eV, rather lower than that given by Richardson et al. [65]. A close inspection of the TOF spectra shows that the $C_5H_3^+$ peak also broadens slightly at this photon energy.

A thermochemical threshold of 21.6 eV [59] has been estimated for the production of CH_3^+ from $C_6H_6^+$, where the reaction involves only a single charge. However, the TOF spectra show no sign of this fragment until the photon energy exceeds the threshold by ∼6 eV. Moreover, the TOF peak shape always appears broad, which suggests that CH_3^+ is being formed through a charge separation reaction. The double ionisation threshold of benzene occurs at 24.6 eV [67], which is ∼3 eV below the observed AE of CH_3^+.

The TOF spectra recorded at high photon energies show that the fragment ion peak shapes alter significantly as the photon energy increases from 31.8 to 35.4 eV. This change in profile is observed most readily in the peaks corresponding to the C_2 and the C_3 groups. In the spectrum recorded at 31.8 eV most of the peaks are well resolved and can be associated with fragments possessing relatively small kinetic energies. However, in the spectrum recorded at 35.4 eV many of the peaks have broadened substantially and must be attributed to fragments possessing initial kinetic energies of several electron volts. Richardson et al. [65] reported appearance energies of 31.3 and 32.2 eV for the charge separation reactions $C_6H_6^{2+} \rightarrow C_2H_3^+ + C_4H_3^+$ and $C_6H_6^{2+} \rightarrow C_3H_3^+ + C_3H_3^+$, respectively. Thus, the observed change in peak shape may be a manifestation of these processes. Further work will be required to substantiate this interpretation.

3.5. Fragmentation rates

Previous work has shown that the unimolecular decay rate $k(E)$ of metastable parent ions can be extracted from an analysis of fragment ion TOF peak shapes [68]. If a parent ion decomposes during the course of acceleration through a TOF spectrometer, then the resulting daughter ion TOF peak profile will be asymmetric. The decay rate may be deduced by

comparing the experimental daughter ion peak profile with the corresponding data obtained by modelling the ion trajectories through the spectrometer. Baer et al. [26] determined decay rates for internal energy selected $C_6H_6^+$ ions by fitting the asymmetric peak profiles of the $C_3H_3^+$ and $C_4H_4^+$ fragments. However, their method involved convoluting an exponential decay curve with a Gaussian function representing the kinetic energy released during dissociation and the thermal motion of the sample. A different approach has been adopted in the present study and relies entirely upon ion trajectory simulations. It is assumed that the metastable ion concentration decays exponentially, and the daughter ion peak shape is obtained by modelling ion trajectories through the TOF spectrometer. This modelling simulates the decomposition of the parent ion into the daughter ion during flight, and also takes into account the initial kinetic energy of the fragment ion.

The total decay rate constant for $C_6H_6^+$ was obtained by modelling the TOF peak shapes for the $C_3H_3^+$ fragments using the SIMION 7 ion optics simulation program [39]. At each photon energy, the computed profiles were compared with the experimental spectra, and the value of k was adjusted to obtain the best fit.

Fragment ions arrive at the detector after a TOF, t, which depends upon the formation times, T, of the daughter ions, since the ions are accelerated towards the detector by the static electric fields of the spectrometer and will experience part of their acceleration as mass 78 ($C_6H_6^+$ ions) and part as mass 39 ($C_3H_3^+$ ions). $T = 0$ is defined as the instant of creation of the $C_6H_6^+$ parent. Those ions which fragment first—and hence experience acceleration forces at the lower mass 39 for the greatest proportion of their flight time—will have the shortest TOF.

Clearly, increments ΔT in the time of the fragment formation do not necessarily equal their equivalent increments, Δt, in the fragment TOF, so that attempting to fit a simple exponential decay curve to the experimental data will not produce the correct experimental value of k. If the relationship between ΔT and Δt were linear, then simple curve fitting could be used to find a value for the apparent rate constant K, from which k could be computed using $K = \alpha k$, where α is a characteristic of the spectrometer [12]. However, since the fields in the spectrometer are not constant, but vary along the ion trajectory, the relationship between K and k is not linear and a not only varies with T, but does so in a non-uniform manner. This difficulty in finding k by fitting an exponential decay to the experimental TOF peak shape has been resolved by using the SIMION program to model the experimental

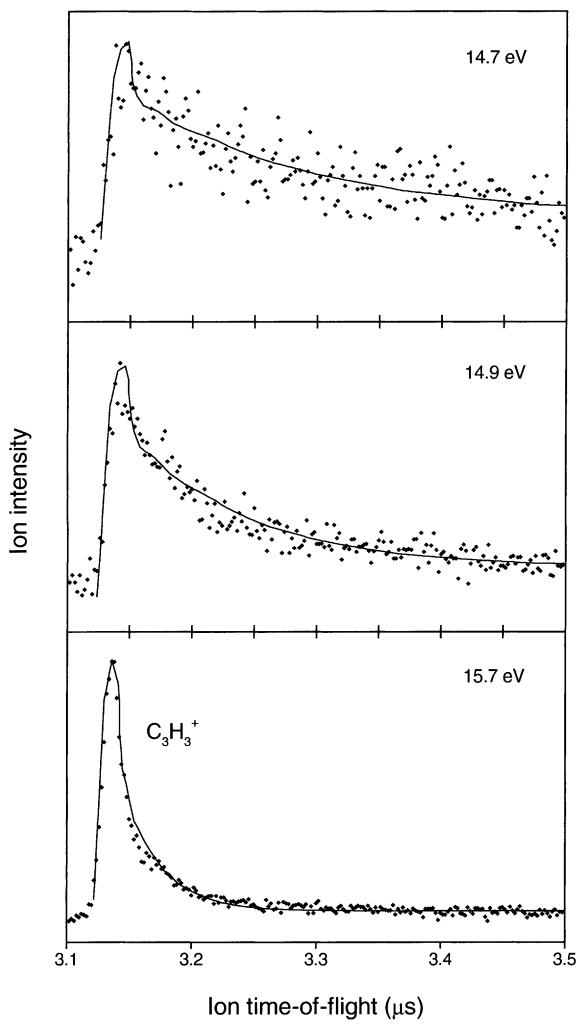

Fig. 11. A comparison between simulated (—) and experimental (···) spectra for the TOF peak associated with the $C_3H_3^+$ fragment, at photon energies of 14.7, 14.9 and 15.7 eV.

apparatus, and to predict the TOF of mass 39 fragments for various values of fragment ion formation time, T.

A SIMION user program was written to create simulated mass 78 ions with a random distribution in a finite source region, delimited by the intersection of the photon beam with the electron detector line of sight, as confirmed in a subsidiary electron flight model. This ensured that only those ions which would be detected in coincidence with photoelectrons were modelled by SIMION. The mass 78 ions were given an initial thermal velocity (corresponding to a kinetic energy of 25 meV) in the direction of the gas jet flow.

After a pre-determined delay (T), input as one of the program parameters, the ion mass was changed, in flight, to 39 amu and a velocity component was added to represent fragmentation with a pre-set kinetic energy in a randomly chosen direction, thus simulating an isotropic ion distribution during fragmentation. Sets of 10,000 ions were flown and the modelled times-of-flight of each set were extracted from the SIMION data file and counted into TOF channels.

The kinetic energy chosen for the fragmenting ions was 10 meV, as this is the most probable kinetic energy for $C_3H_3^+$ ions from the fragmentation of metastable $C_6H_6^+$ [69]. This energy also provided a good agreement between the rise times of the modelled peaks and those of the experimental TOF peaks.

The modelling was carried out for $T = 0$ ns to $T = 1000$ ns, using increments of 25 ns, with one set of 10,000 ions being processed at each formation time. Each resulting TOF data set was weighted by an exponential decay factor, $m(T)$, such that

$$m(T) = \mathrm{e}^{-kT}$$

The weighted data were then summed and plotted against TOF, k being varied to find the best fit to the experimental data for each photon energy. Uncertain-

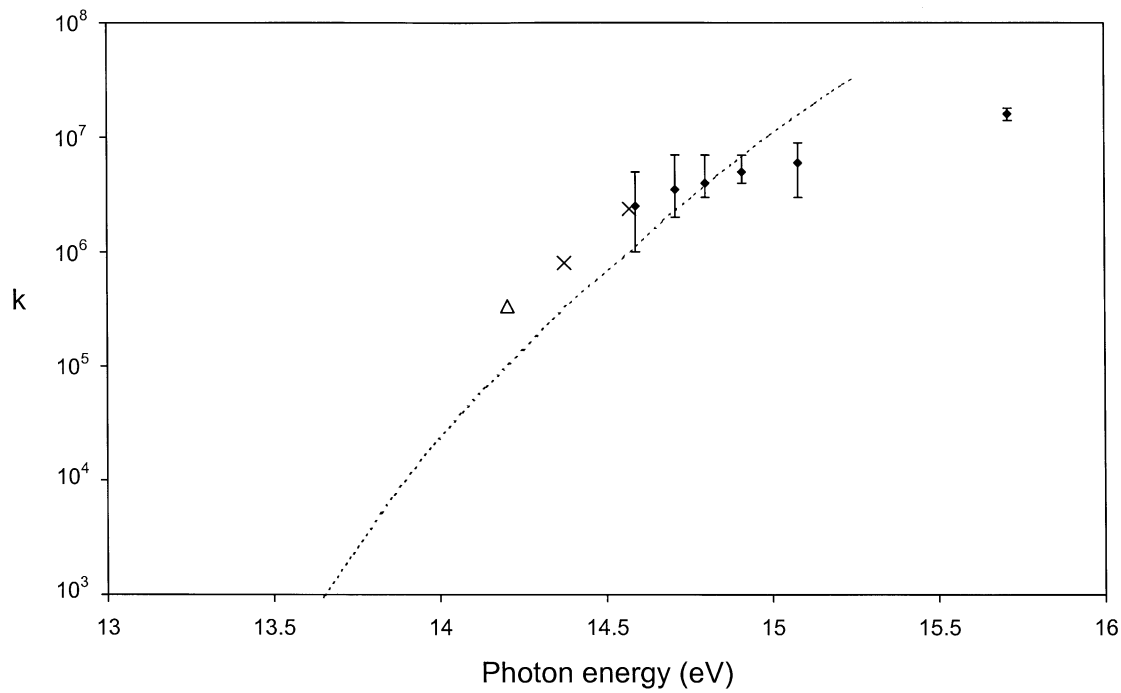

Fig. 12. Total decay rate of $C_6H_6^+$ as a function of photon energy. Key to data: (◆) present data, (×) Eland and Schulte [22], (△) Baer et al. [26], (- - -) Neusser [7].

ties in the fit were estimated by varying k until the fit became unacceptable. Fig. 11 shows examples of experimental and simulated spectra at three photon energies.

Since the time increments used in the exponential weighting are increments in the formation time, T, and not in the measured TOF, t, the problem of mapping from T to t is negated. In addition, the model takes into account the effect on peak shape of a source region of discrete volume, rather than approximating it to a point source, as is the case with a simple exponential curve fit. The sharp changes in slope in the modelled decay curves (seen, for example, in Fig. 11 around 3.17 μs), illustrate the effect of the non-uniformity of $\alpha(T)$, which is especially pronounced at low T. As $\alpha(T)$ changes, the apparent rate constant $K = \alpha(T)k$ changes accordingly and so the shape of the curve deviates from that of a straightforward exponential decay. The SIMION modelling shows that equally spaced increments in the formation time, T, produce varying increments in t when T is in the range 0–100 ns, but produce almost equal increments in t when T lies between 100 and 800 ns. This results in the longer formation times producing a smoother decay curve.

The total rate constants derived from the present $C_3H_3^+$ peak fitting procedure, and those deduced by Eland and Schulte [22], and by Baer et al. [26] are plotted in Fig. 12 together with the theoretical curve calculated by Neusser [7]. Photoelectron spectroscopy studies indicate that at a photon energy of 15 eV the ground and the first four excited ionic states are populated [70]. However, Neusser [7] has calculated a threshold energy of 4.19 eV for the fragmentation channel leading to $C_3H_3^+$ production. Therefore, energy considerations suggest that at $h\nu = 15$ eV, only benzene ions formed initially in the $\tilde{C}^2E_{1u}$ or the $\tilde{D}^2B_{2u}$ states are likely to fragment to form $C_3H_3^+$ ions. In addition, since the decay rate falls rapidly as the ion internal energy decreases [7], the $C_3H_3^+$ TOF peak shape will be dominated by fragmentation from benzene parent ions formed in photoionisation processes where very little kinetic energy is carried away by the electron.

Acknowledgements

We are grateful for financial support and a CASE studentship (L.C.) from the EPSRC, and for a Visiting Fellowship (L.G.S.) from the Royal Society.

References

[1] T. Baer, W.L. Hase, Unimolecular Reaction Dynamics: Theory and Experiments, Oxford University Press, New York, 1996.
[2] C.Y. Ng, in: T. Baer, C.Y. Ng, I. Powis (Eds.), The Structure, Energetics and Dynamics of Organic Ions, Wiley, Chichester, 1996.
[3] T. Baer, Int. J. Mass Spectrom. 200 (2000) 443.
[4] W. Forst, Theory of Unimolecular Reactions, Academic Press, New York, 1973.
[5] J.H. Beynon, J.R. Gilbert, Application of Transition State Theory to Unimolecular Reactions, Wiley, Chichester, 1984.
[6] R.G. Gilbert, S.C. Smith, Theory of Unimolecular and Recombination Reactions, Blackwell Scientific, Oxford, 1990.
[7] H.J. Neusser, J. Phys. Chem. 93 (1989) 3897.
[8] G.K. Jarvis, K.-M. Weitzel, M. Malow, T. Baer, Y. Song, C.Y. Ng, Rev. Sci. Instrum. 70 (1999) 3892.
[9] R. Stockbauer, Int. J. Mass Spectrom. Ion Phys. 25 (1977) 89.
[10] D.M.P. Holland, D.A. Shaw, I. Sumner, M.A. Hayes, R.A. Mackie, B. Wannberg, L.G. Shpinkova, E.E. Rennie, L. Cooper, C.A.F. Johnson, J.E. Parker, Nucl. Instrum. Meth. B179 (2001) 436.
[11] E.E. Rennie, L. Cooper, C.A.F. Johnson, J.E. Parker, R.A. Mackie, L.G. Shpinkova, D.M.P. Holland, D.A. Shaw, M.A. Hayes, Chem. Phys. 263 (2001) 149.
[12] D. Proch, D.M. Rider, R.N. Zare, Chem. Phys. Lett. 81 (1981) 430.
[13] J.W. Keister, T. Baer, R. Thissen, C. Alcaraz, O. Dutuit, H. Audier, V. Troude, J. Phys. Chem. A102 (1998) 1090.
[14] F. Güthe, M. Malow, K.-M. Weitzel, H. Baumgärtel, Int. J. Mass Spectrom. Ion. Process. 172 (1998) 47.
[15] D.A. Shaw, D.M.P. Holland, M.A. MacDonald, M.A. Hayes, L.G. Shpinkova, E.E. Rennie, C.A.F. Johnson, J.E. Parker, W. von Niessen, Chem. Phys. 230 (1998) 97.
[16] E.E. Rennie, C.A.F. Johnson, J.E. Parker, D.M.P. Holland, D.A. Shaw, M.A. MacDonald, M.A. Hayes, L.G. Shpinkova, Chem. Phys. 236 (1998) 365.
[17] E.E. Rennie, C.A.F. Johnson, J.E. Parker, R. Ferguson, D.M.P. Holland, D.A. Shaw, Chem. Phys. 250 (1999) 217.
[18] L. Cooper, L.G. Shpinkova, E.E. Rennie, D.M.P. Holland, D.A. Shaw, Int. J. Mass Spectrom. 207 (2001) 223.
[19] E.E. Rennie, C.A.F. Johnson, J.E. Parker, D.M.P. Holland, D.A. Shaw, M.A. Hayes, Chem. Phys. 229 (1998) 107.
[20] H.M. Rosenstock, J. Dannacher, J.F. Liebman, Radiat. Phys. Chem. 20 (1982) 7.
[21] B. Andlauer, Ch. Ottinger, Z. Naturforsch. 27a (1972) 293.
[22] J.H.D. Eland, H. Schulte, J. Chem. Phys. 62 (1975) 3835.
[23] J.H.D. Eland, R. Frey, H. Schulte, B. Brehm, Int. J. Mass Spectrom. Ion Phys. 21 (1976) 209.

[24] H.M. Rosenstock, J.T. Larkins, J.A. Walker, Int. J. Mass Spectrom. Ion Phys. 11 (1973) 309.
[25] H.M. Rosenstock, K.E. McCulloh, F.P. Lossing, Int. J. Mass Spectrom. Ion Phys. 25 (1977) 327.
[26] T. Baer, G.D. Willett, D. Smith, J.S. Phillips, J. Chem. Phys. 70 (1979) 4076.
[27] W.J. van der Hart, Int. J. Mass Spectrom. Ion Process. 130 (1994) 173.
[28] O. Braitbart, S. Tobita, P. Roy, I. Nenner, P. Lablanquie, D.A. Hagan, S. Leach, Int. J. Mass Spectrom. Ion Process. 124 (1993) 185.
[29] H. Kühlewind, H.J. Neusser, E.W. Schlag, J. Phys. Chem. 88 (1984) 6104.
[30] H. Kühlewind, A. Kiermeier, H.J. Neusser, J. Chem. Phys. 85 (1986) 4427.
[31] H. Kühlewind, A. Kiermeier, H.J. Neusser, E.W. Schlag, J. Chem. Phys. 87 (1987) 6488.
[32] S.J. Klippenstein, J.D. Faulk, R.C. Dunbar, J. Chem. Phys. 98 (1993) 243.
[33] Th.L. Grebner, H.J. Neusser, Int. J. Mass Spectrom. 185–187 (1999) 517.
[34] M.S. Kim, C.H. Kwon, J.C. Choe, J. Chem. Phys. 113 (2000) 9532.
[35] K.R. Jennings, Z. Naturforsch. 22a (1967) 454.
[36] A. Fraefel, J. Seibl, Int. J. Mass Spectrom. Ion Phys. 51 (1983) 245.
[37] R. Weinkauf, K. Walter, C. Weickhardt, U. Boesl, E.W. Schlag, Z. Naturforsch. 44a (1989) 1219.
[38] D.M.P. Holland, J.B. West, A.A. MacDowell, I.H. Munro, A.G. Beckett, Nucl. Instrum. Meth. B44 (1989) 233.
[39] D.A. Dahl, Int. J. Mass Spectrom. 200 (2000) 3.
[40] W.C. Wiley, I.H. McLaren, Rev. Sci. Instrum. 26 (1955) 1150.
[41] G. Cooper, Y. Zheng, G.R. Burton, C.E. Brion, Rev. Sci. Instrum. 64 (1993) 1140.
[42] NIST Chemistry Webbook Standard Reference Database, Number 69, February 2000 Release, and the NIST Standard Reference Database 19A.
[43] C. Lifshitz, A.M. Peers, M. Weiss, M.J. Weiss, Adv. Mass Spectrom. 6 (1974) 871.
[44] Yu.L. Sergeev, M.E. Akopyan, F.I. Vilesov, V.I. Kleimenov, Opt. Spectrosc. 29 (1970) 63.
[45] P. Natalis, J.L. Franklin, J. Phys. Chem. 69 (1965) 2935.
[46] C. Lifshitz, B.G. Reuben, J. Chem. Phys. 50 (1969) 951.
[47] A. Hustrulid, P. Kusch, J.T. Tate, Phys. Rev. 54 (1938) 1037.
[48] J. Olmsted, K. Street, A.S. Newton, J. Chem. Phys. 40 (1964) 2114.
[49] S.W. Staley, T.D. Norden, J. Am. Chem. Soc. 111 (1989) 445.
[50] S.J. Klippenstein, Int. J. Mass Spectrom. Ion Phys. 167/168 (1997) 235.
[51] J. Hrusak, D. Schröder, S. Iwata, J. Chem. Phys. 106 (1997) 7541.
[52] A. Nicolaides, D.M. Smith, F. Jensen, L. Radom, J. Am. Chem. Soc. 119 (1997) 8083.
[53] G. Koster, W.J. van der Hart, Int. J. Mass Spectrom. Ion Process. 163 (1997) 169.
[54] W.J. van der Hart, Int. J. Mass Spectrom. 176 (1998) 23.
[55] P. Ausloos, J. Am. Chem. Soc. 103 (1981) 3931.
[56] W. Wagner-Redeker, A.J. Illies, P.R. Kemper, M.T. Bowers, J. Am. Chem. Soc. 105 (1983) 5719.
[57] M.-Y. Zhang, B.K. Carpenter, F.W. McLafferty, J. Am. Chem. Soc. 113 (1991) 9499.
[58] W.J. van der Hart, Int. J. Mass Spectrom. Ion Process. 171 (1997) 269.
[59] F. Rebentrost, A. Ben-Shaul, J. Chem. Phys. 74 (1981) 3255.
[60] H.W. Jochims, E. Rühl, H. Baumgärtel, S. Tobita, S. Leach, Int. J. Mass Spectrom. Ion Process. 167/168 (1997) 35.
[61] H.W. Jochims, H. Baumgärtel, S. Leach, Astron. Astrophys. 314 (1996) 1003.
[62] T.A. Carlson, P. Gerard, M.O. Krause, F.A. Grimm, B.P. Pullen, J. Chem. Phys. 86 (1987) 6918.
[63] B.P. Mathur, E.M. Burgess, D.E. Bostwick, T.F. Moran, Org. Mass Spectrom. 16 (1981) 92.
[64] B. Brehm, U. Fröbe, H.-P. Neitzke, Int. J. Mass Spectrom. Ion Phys. 57 (1984) 91.
[65] P.J. Richardson, J.H.D. Eland, P. Lablanquie, Org. Mass Spectrom. 21 (1986) 289.
[66] K. Codling, L.J. Frasinski, Contemporary Phys. 35 (1994) 243.
[67] R.I. Hall, L. Avaldi, G. Dawber, A.G. McConkey, M.A. MacDonald, G.C. King, Chem. Phys. 187 (1994) 125.
[68] T. Baer, in: M.T. Bowers (Ed.), Gas Phase Ion Chemistry, Vol. 1, Academic Press, New York, 1979.
[69] M.F. Jarrold, W. Wagner-Redeker, A.J. Illies, N.J. Kirchner, M.T. Bowers, Int. J. Mass Spectrom. Ion Phys. 58 (1984) 63.
[70] P. Baltzer, L. Karlsson, B. Wannberg, G. Öhrwall, D.M.P. Holland, M.A. MacDonald, M.A. Hayes, W. von Niessen, Chem. Phys. 224 (1997) 95.